# OT Score: An OT based Confidence Score for Unsupervised Domain Adaptation

Yiming Zhang<sup>1</sup> Sitong Liu<sup>2</sup> Alex Cloninger<sup>1\*</sup>

<sup>1</sup>University of California, San Diego <sup>2</sup>University of Washington {yiz134, acloninger}@ucsd.edu, sitongl@uw.edu

### **Abstract**

We address the computational and theoretical limitations of existing distributional alignment methods for unsupervised domain adaptation (UDA), particularly regarding the estimation of classification performance and confidence without target labels. Current theoretical frameworks for these methods often yield computationally intractable quantities and fail to adequately reflect the properties of the alignment algorithms employed. To overcome these challenges, we introduce the Optimal Transport (OT) score, a confidence metric derived from a novel theoretical analysis that exploits the flexibility of decision boundaries induced by Semi-Discrete Optimal Transport alignment. The proposed OT score is intuitively interpretable, theoretically rigorous, and computationally efficient. It provides principled uncertainty estimates for any given set of target pseudo-labels without requiring model retraining, and can flexibly adapt to varying degrees of available source information. Experimental results on standard UDA benchmarks demonstrate that classification accuracy consistently improves by identifying and removing low-confidence predictions, and that OT score significantly outperforms existing confidence metrics across diverse adaptation scenarios.

### 1 Introduction

In recent years, deep neural networks have achieved remarkable breakthroughs across a wide range of applications. However, if the distribution of the training and test data differs, significant performance degradation occurs, which is known as a domain shift [29], which makes retraining critical for the model to re-gain the generalization ability in new domains.

Unsupervised domain adaptation (UDA) mitigates the domain shift problem where only unlabeled data is accessible in the target domain [9]. A key approach for UDA is aligning the distributions of both domains by mapping data to a shared latent feature space. Consequently, a classifier trained on source domain features in this space can generalize well to the target domain. Several existing works [16], [17], [4], [3], [25] exhibits a principled way to transform target distribution to be 'closer' to the source distribution so that the classifier learned from the source data can be directly applied to the target domain thus pseudo-labels (or predictions) can be made accordingly.

This leads to the question of whether such transformations from the target to the source distribution can accurately match the corresponding class-conditional distributions. For any given target dataset, it is always possible to align its feature distribution with that of the source domain using a divergence function, regardless of whether classes overlap. However, performing UDA in this way is reasonable only if target features remain well-separated by the decision boundaries induced through alignment in the latent feature space—something that is typically difficult to determine in practice. Moreover, the distributional alignment approach complicates the identification of samples with low-confidence

<sup>\*</sup>Corresponding author.

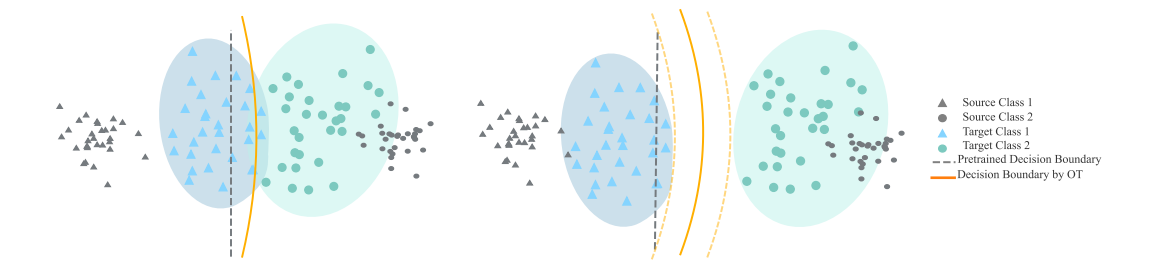


Figure 1: (Left) Overlapping clusters. (Right) Separated clusters with flexible decision boundaries.

pseudo-labels (i.e., samples close to overlapping regions), potentially causing noisy supervision and thus degrading classification performance. This issue becomes particularly critical when no labeled information for the target data is available. To address these challenges, we will focus on the following two questions in this work:

Question 1: What kind of domain shift can be aligned back with the source distribution while preserving the correct class labels?

Question 2: Is there a theoretically guaranteed confidence score that can be used to evaluate the uncertainty of given pseudo-labels?

To answer these questions, it is necessary to specify which distance is used for the distributional alignment since the pulling strategy on the target varies according to the divergence used. Optimal Transport (OT) distance is a popular distance adopted in UDA problems [4], [3], [25]. Using OT distance has an intuitive interpretation since it considers the overall geometry of data. Redko et al. [23] provides a theoretical guarantee connecting generalization errors on source and target domains based on the Wasserstein distance, which validates the idea of minimizing Wasserstein distance between source and target distributions:

**Theorem 1** (Informal [23]). Under certain assumptions, with probability at least  $1 - \delta$  for all hypothesis h and  $\varsigma' < \sqrt{2}$  the following holds:

$$\epsilon_{\mathcal{T}}(h) \le \epsilon_{\mathcal{S}}(h) + W_1(\hat{\mu}_{\mathcal{S}}, \hat{\mu}_{\mathcal{T}}) + \sqrt{2\log\left(\frac{1}{\delta}\right)/\varsigma'}\left(\sqrt{\frac{1}{N_{\mathcal{S}}}} + \sqrt{\frac{1}{N_{\mathcal{T}}}}\right) + \lambda$$

where  $\lambda$  is the combined error of the ideal hypothesis  $h^*$  that minimizes the combined error of  $\epsilon_{\mathcal{S}}(h) + \epsilon_{\mathcal{T}}(h)$ .

Despite its advantages, the theoretical understanding of label-preserving alignment under OT loss remains underexplored. A bad pulling strategy on  $\mathcal{T}$  might minimize  $W_1$  term to 0 without any guarantee for the  $\lambda$  term in the feature space. We address this theoretical gap in Section 4.1, thereby answering Question 1.

Guided by our theoretical analysis under the semi-discrete OT framework (Section 4.2), we address Question 2 by introducing the **OT score**—a confidence metric designed to quantify uncertainty in pseudo-labeled target samples. As illustrated in Figure 1, the OT score reflects the flexibility of decision boundaries induced by semi-discrete OT alignment, which enables effective uncertainty estimation in the target domain. This allows the algorithm to abstain from classifying samples with high uncertainty. Compared to fully continuous or fully discrete OT formulations, semi-discrete OT is computationally more efficient, especially in high-dimensional spaces and large-scale datasets. It provides a flexible framework that can be readily adapted to scenarios with limited source information (e.g., cases where only class-wise mean features from the source are available). Such scenarios are practical and realistic in real-world applications, as they facilitate the use of source information while preserving privacy and minimizing computational and storage overhead. Furthermore, our method is compatible with pseudo labels generated by state-of-the-art DA methods, which may also leverage partial source-domain information. A detailed comparison with existing confidence scores is provided in Section 2.

#### **Contributions:**

- We provide theoretical justifications about allowed distribution shifts in order to have a label-preserving OT.
- We define a novel confidence score, the OT score, which is theoretically interpretable and accounts for the geometry induced by OT alignment between the source and target distributions.
- Experimental results demonstrate that filtering out low-confidence predictions consistently improves classification accuracy, and that the proposed OT score significantly outperforms existing confidence metrics across diverse pseudo-labeling strategies.

**Notation**. Given any probability measure  $\mu$  and a measurable map T between measurable spaces,  $T: \mathcal{X} \longrightarrow \mathcal{Y}$ , we denote  $T_{\#}\mu$  the pushforward measure on  $\mathcal{Y}$  which is characterized by  $(T_{\#}\mu)(A) = \mu\left(T^{-1}(A)\right)$  for measurable set A. Let  $\hat{\mu}$  denote the corresponding empirical measure  $\frac{1}{N}\sum_{i=1}^N \delta_{x_i}$  where  $x_i$  are i.i.d. samples from  $\mu$ . We also write  $x \in \hat{\mu}$  to indicate  $x \in \{x_i\}_{i=1}^N$ . If not otherwise specified,  $\|\cdot\|$  represents the Euclidean norm.

### 2 Related Works

Theory about DA: Several theoretical works have investigated the learnability and generalization guarantees of domain adaptation (DA). Specifically, [1] analyzes the DA learnability problem and sample complexity under the standard VC-dimension framework, and identifies a setting in which no algorithm can successfully solve the DA problem. In a related direction, [24] provides a theoretical analysis about the existence of a hypothesis that performs well across both source and target domains, and further establishes finite-sample approximation properties of the  $\lambda$  term. A closely related theoretical work is [14], which alleviates the label mismatching problem by searching for a transformation T that satisfies the following conditions: (1)  $T_{\#}\mu_S = \mu_T$ , and (2) T preserves the labels.

Confidence Scores: Uncertainty estimation and confidence score have been prevalently employed in machine learning to improve model robustness. In particular, ordinal ranking techniques have been commonly used for selective classification ([13]; [6]; [19]; [20]), where the goal is to prioritize or filter samples based on their confidence scores in order to exclude low-confidence samples during training. Lee et al. [15] propose the JMDS score to effectively identify low-confidence samples, thereby enhancing the reliability of the DA process. However, most existing confidence scores rely primarily on cluster-level information in the feature space, without explicitly modeling the geometric relationship between domains. In contrast, our proposed OT score take into account the geometry induced by the OT map, establishing a stronger connection between the source and target domains when computing confidence scores.

### 3 Optimal Transport and Domain Adaptation

In this section, we first present the domain adaptation problem. Then we give necessary backgrounds of optimal transport.

### 3.1 Domain Adaptation

Let  $\Omega\subseteq\mathbb{R}^d$  be the sample space and  $\mathcal{P}(\Omega)$  be the set of all probability measures over  $\Omega$ . In a general supervised learning paradigm for classification problems, we have a labeling function  $f_{\boldsymbol{\theta}^*}:\mathbb{R}^d\to\mathbb{R}^k$  obtained from a parametric family  $f_{\boldsymbol{\theta}}$  by training on a set of points  $\mathbf{X}^{\mathcal{S}}=\{x_1^{\mathcal{S}},...,x_{N^{\mathcal{S}}}^{\mathcal{S}}\}$  sampled from a source distribution  $\mathbf{P}_{\mathcal{S}}\in\mathcal{P}(\Omega)$  and corresponding one-hot encoded labels  $\mathbf{Y}^{\mathcal{S}}=\{y_1^{\mathcal{S}},...,y_{N^{\mathcal{S}}}^{\mathcal{S}}\}$ .

Let  $\mathbf{X}^{\mathcal{T}} = \{x_1^{\mathcal{T}}, ..., x_{N^{\mathcal{T}}}^{\mathcal{T}}\}$  be a dataset sampled from a target distribution  $\mathbf{P}_{\mathcal{T}} \in \mathcal{P}(\Omega)$  without label information. The difference between  $\mathbf{P}_{\mathcal{S}}$  and  $\mathbf{P}_{\mathcal{T}}$  may lead to a poor performance if we use  $f_{\theta^*}$  for the new classification problem. In order to overcome the challenge of distributional shift, a common way is to decompose a neural network  $f_{\theta}$  into a feature mapping  $\phi_v$  composed with a classifier  $h_w$  such that  $f_{\theta} = h_w \circ \phi_v$ , followed by minimizing the distance between  $(\phi_{v^*})_{\#} \mathbf{P}_{\mathcal{S}}$  and  $(\phi_v)_{\#} \mathbf{P}_{\mathcal{T}}$  so that the target distribution will be aligned with the source distribution in the feature space. Then we may classify (or assign pseudo labels to) target data points based on the optimization result in

the feature space. Various choices of divergence objective  $D((\phi_{\boldsymbol{v}^*})_{\#}\mathbf{P}_{\mathcal{S}},(\phi_{\boldsymbol{v}})_{\#}\mathbf{P}_{\mathcal{T}})$  can be utilized. In this work, we focus on the distributional alignment between  $(\phi_{\boldsymbol{v}^*})_{\#}\mathbf{P}_{\mathcal{S}}$  and  $(\phi_{\boldsymbol{v}})_{\#}\mathbf{P}_{\mathcal{T}}$  using Wasserstein distance.

### 3.2 Optimal Transport

### 3.2.1 General Theory of OT

Given two probability distributions  $\mu, \nu \in \mathcal{P}(\mathbb{R}^d)$ , the Wasserstein-p distance for  $p \in [1, +\infty]$  is defined by

$$W_p(\mu, \nu) := \left( \min_{\gamma \in \Gamma(\mu, \nu)} \int_{\mathbb{R}^d \times \mathbb{R}^d} \|x - y\|^p d\gamma \right)^{\frac{1}{p}},$$

where  $\Gamma(\mu, \nu)$  is the collection of all couplings of  $\mu$  and  $\nu$ . The optimization problem

$$\min_{\gamma \in \Gamma(\mu,\nu)} \int_{\mathbb{R}^d \times \mathbb{R}^d} \|x - y\|^p d\gamma \tag{KP}$$

is referred as the Kantorovitch problem in optimal transport. It is shown by Kantorovich–Rubinstein Duality theorem that (KP) has a dual form [26]:

Theorem 2 (Kantorovich-Rubinstein Duality).

$$\min_{(KP)} = \sup \Big\{ \int_{\mathbb{R}^d} \phi(x) \, d\mu + \int_{\mathbb{R}^d} \psi(y) \, d\nu : (\phi, \psi) \in Lip_b(\mathbb{R}^d) \times Lip_b(\mathbb{R}^d), \ \phi(x) + \psi(y) \le \|x - y\|^p \Big\}.$$

In addition, when the supremum in the dual formulation is a maximum, the optimal value is attained at a pair  $(\phi, \phi^c)$  with  $\phi$ ,  $\phi^c$  bounded and Lipschitz, where  $\phi^c(y) := \inf_{x \in \mathbb{R}^d} ||x - y||^p - \phi(x)$ .

With the dual problem introduced, [2] proves Brenier's theorem, which gives a sufficient condition under which the minimizer of the optimal transport problem is unique and is induced by a map  $T = \nabla \phi$  for some convex function  $\phi$ , i.e. the OT map exists.

Under mild conditions on  $\mu$  and  $\nu$ , Brenier's theorem is satisfied when  $c(x,y) = ||x-y||_p$  for p > 1. Although there is no guarantee about uniqueness of the optimal transport map when p = 1, the existence of an optimal transport map can be proved through a secondary variational problem [26]:

**Theorem 3** (Existence of optimal transport map when p=1). Let  $O(\mu,\nu)$  be the optimal transport plans for the cost ||x-y|| and denote by  $K_p$  the functional associating to  $\gamma \in \mathcal{P}(\Omega \times \Omega)$ , the quantity  $\int ||x-y||^p d\gamma$ . Under the usual assumption  $\mu \ll \mathcal{L}^d$ , the secondary variational problem

$$\min \{K_2(\gamma) : \gamma \in O(\mu, \nu)\}\$$

admits a unique solution  $\bar{\gamma}$ , which is induced by a transport map T.

#### 3.2.2 Semi-discrete Optimal Transport

A special case of interest is when  $\nu = \sum_{j=1}^{m} b_j \delta_{y_j}$  is a discrete probability measure. Adapting the duality result to this setting, we have

$$W_p^p(\mu,\nu) = \max_{\boldsymbol{w} \in \mathbb{R}^m} \int_{\mathbb{R}^d} \boldsymbol{w}^c(x) d\mu + \sum_{j=1}^m w_j b_j,$$

and in this case,  $w^{c}(x) := \min_{i} ||x - y_{i}||^{p} - w_{i}$ .

We can define a disjoint decomposition of the whole space using the Laguerre cells associated to the dual weights w:

$$\mathbb{L}_{\boldsymbol{w}}(y_j) := \Big\{ x \in \mathbb{R}^d : \forall j' \neq j, \|x - y_j\|^p - w_j \le \|x - y_{j'}\|^p - w_{j'} \Big\}.$$

Then

$$W_p^p(\mu,\nu) = \max_{\boldsymbol{w} \in \mathbb{R}^m} \sum_{j=1}^m \int_{\mathbb{L}_{\boldsymbol{w}}(y_j)} (\|x - y_j\|^p - w_j) d\mu + \langle \boldsymbol{w}, \boldsymbol{b} \rangle.$$

The optimization problem above can be solved by (stochastic) gradient ascent methods since the j-th entry of gradient for the objective function can be computed via  $b_j - \int_{\mathbb{L}_{\boldsymbol{w}}(y_j)} d\mu$ . Once the optimal vector  $\boldsymbol{w}$  is computed, the optimal transport map  $T^{\nu}_{\mu}$  simply maps  $x \in \mathbb{L}_{\boldsymbol{w}}(y_j)$  to  $y_j$  [22]. Also, it can be shown such OT map is unique under mild assumptions [10], [8]. In the rest of the paper, for any  $x \in \operatorname{supp} \mu$  and  $y_j \in \operatorname{supp} \nu$ , we denote  $\tilde{d}_{\boldsymbol{w}}(x,y_j) := \|x-y_j\|^p - w_j$ .

### 4 Theoretical Analysis

In this section, we present theoretical insights into the use of OT for addressing DA problems. Complete proofs of all theoretical results are provided in Appendix B. For clarity and tractability, we focus on binary classification tasks. As discussed in Section 3.1, our interest lies in neural network—based DA. To this end, we adopt assumptions inspired by Neural Collapse [12], a prevalent phenomenon observed in well-trained neural networks. The extent to which the target feature distribution conforms to the Neural Collapse structure depends on the severity of the distributional shift between the source and target domains.

Remark 1 (Neural Collapse). Neural collapse (NC) is a phenomenon observed in well-trained neural networks where the learned features of samples belonging to the same class converge to a single point or form tightly clustered structures in the feature space, while the features of different classes become maximally separated. NC emerges while training modern classification DNNs past zero error to further minimize the loss [21]. During NC, the class means of the DNN's last-layer features form a symmetric structure with maximal separation angle, while the features of each individual sample collapse to their class means. This simple structure of the feature layer not only appears beneficial for generalization but also helps in transfer learning and adversarial robustness. There are three main theoretical frameworks proposed to explain the emergence of NC: "Unconstrained Features Model" [18], [28], [11], "Local Elasticity" [31] and "Neural (Tangent Kernel) Collapse" [27].

In the following subsection, we focus on the setting where the class-conditional distributions in both the source and target domains are supported on, or concentrated within, bounded subsets of the feature space. Under this assumption, we analyze how data clusters are transported by the OT map.

#### 4.1 Sufficient Conditions for Correct Classification

We begin by presenting a necessary condition on the target data distribution under which correct classification can be expected after applying optimal transport. The following theorem quantifies the relationship between the probability of misclassification and the concentration properties of class-conditional distributions. Intuitively, if each class distributions is concentrated within a bounded region and these regions are well-separated across classes, classification results after OT map will be correct with high probability.

**Theorem 4.** Suppose for each of the probability measures  $\mu_i$ ,  $\nu_i$  there exist disjoint bounded sets  $E_{\mu_i}(or\ E_{\nu_i})$  such that  $\mu_i(E_{\mu_i}) \geq 1 - \epsilon$  and  $(r_{\mu_1} + r_{\nu_1} + l_1) + (r_{\mu_2} + r_{\nu_2} + l_2) < L_1 + L_2$ , where  $r_{\mu_i}(or\ r_{\nu_i})$  is the diameter of  $E_{\mu_i}(or\ E_{\nu_i})$ ,  $l_i = d(E_{\mu_i}, E_{\nu_i})$ ,  $L_1 = d(E_{\mu_1}, E_{\nu_2})$ ,  $L_2 = d(E_{\mu_2}, E_{\nu_1})$ . Assume further that  $E_{\nu_1}$  and  $E_{\nu_2}$  are correctly separated by the trained classifier. Then with probability greater than  $1 - 7\epsilon$ , target samples will be correctly classified after the optimal transportation  $T^\mu_\nu$ .

**Remark 2.** Our concentration assumption applies to various probability distributions including subgaussian distributions.

The proof is based on the intuitive observation from the following lemma:

**Lemma 5.** Suppose we have probability measures  $\mu_i$  and  $\nu_i$  with bounded support. Also assume  $\operatorname{supp} \mu_1$  and  $\operatorname{supp} \mu_2$  are disjoint,  $\operatorname{supp} \nu_1$  and  $\operatorname{supp} \nu_2$  are disjoint. Let  $r_{\mu_i}$  denote the diameter of the support of  $\mu_i$  and set  $l_i = d(\operatorname{supp} \mu_i, \operatorname{supp} \nu_i)$ ,  $L_1 = d(\operatorname{supp} \mu_1, \operatorname{supp} \nu_2)$ ,  $L_2 = d(\operatorname{supp} \mu_2, \operatorname{supp} \nu_1)$ . Suppose  $\mu := \frac{1}{2}\mu_1 + \frac{1}{2}\mu_2$ ,  $\nu := p\nu_1 + (1-p)\nu_2$  for some  $p \in (0, \frac{1}{2}]$ . If  $(r_{\mu_1} + r_{\nu_1} + l_1) + (r_{\mu_2} + r_{\nu_2} + l_2) < L_1 + L_2$ , then  $T^{\mu}_{\nu}(\operatorname{supp} \nu_1) \subset \operatorname{supp} \mu_1$  up to a  $\nu$  negligible set

Table 1: Evaluation	of confidence scores	based on AURC (DSAN).

Dataset	Task	Maxprob	Ent	Cossim	JMDS	OT Score
	$Ar \to Cl$	0.4306	0.4284	0.4170	0.4515	0.3403
	$Ar \rightarrow Pr$	0.2745	0.2738	0.2512	0.2849	0.2133
	$\text{Ar} \rightarrow \text{Rw}$	0.1469	0.1493	0.1521	0.1860	0.1157
	$Cl \rightarrow Ar$	0.2600	0.2631	0.2340	0.3228	0.2097
	$Cl \rightarrow Pr$	0.1757	0.1777	0.1612	0.2225	0.1503
Office-Home	$Cl \rightarrow Rw$	0.1834	0.1848	0.1865	0.2246	0.1493
Office-Hoffie	$\text{Pr} \rightarrow \text{Ar}$	0.2371	0.2381	0.2245	0.2776	0.1984
	$\text{Pr} \to \text{Cl}$	0.3139	0.3105	0.3149	0.3302	0.2711
	$\text{Pr} \rightarrow \text{Rw}$	0.0974	0.0992	0.1037	0.1250	0.0817
	$Rw \to Ar$	0.1301	0.1318	0.1268	0.1751	0.1023
	$Rw \to Cl$	0.2581	0.2555	0.2641	0.2718	0.2112
	$Rw \to Pr$	0.0681	0.0684	0.0628	0.1026	0.0561
	Avg.	0.2146	0.2150	0.2082	0.2478	0.1749
VisDA-2017	$T\toV$	0.2301	0.2290	0.2289	0.2296	0.1799

#### 4.2 Post-check and OT Score

Although results in Section 4.1 provide valuable theoretical insights into OT alignment, they remain difficult to compute or verify in practical settings. In this section, we leverage the semi-discrete OT formulation to derive an equivalent condition for perfect classification under OT alignment. Building upon this, we introduce a novel quantity, OT score, that can be utilized in practice to post-check the performance of the classification from distributional alignment based DA algorithms. Also, we will show later how the following theorem inspires a way to recognize target data points classified with low confidence.

**Theorem 6.** Suppose  $\mu$  and  $\nu$  are compactly supported. Then  $(T_{\nu}^{\hat{\mu}})_{\#}\nu_{1} = \hat{\mu}_{1}$  and  $(T_{\nu}^{\hat{\mu}})_{\#}\nu_{2} = \hat{\mu}_{2}$  if and only if

$$\sup_{x\in\nu_1}\max_{z\in\hat{\mu}_2}\min_{y\in\hat{\mu}_1}\tilde{d}_{\boldsymbol{w}}(x,y)-\tilde{d}_{\boldsymbol{w}}(x,z)\leq 0\leq \inf_{x\in\nu_2}\max_{z\in\hat{\mu}_2}\min_{y\in\hat{\mu}_1}\tilde{d}_{\boldsymbol{w}}(x,y)-\tilde{d}_{\boldsymbol{w}}(x,z),$$

where d is defined as in Section 3.2.2

With  $\mu$  being the source measure and  $\nu$  being the target measure, we define a new function  $g(x) := \max_{z \in \hat{\mu}_2} \min_{y \in \hat{\mu}_1} \tilde{d}(x,y) - \tilde{d}(x,z)$ . Hence, the g value gap  $\inf_{x \in \nu_2} g(x) - \sup_{x \in \nu_1} g(x)$  reflects the flexibility of a classification boundary induced by semi-discrete OT and a larger g value gap implies better classification performance. See Figure 1 for a visual illustration.

In practice, this g value gap can be used as a post-check tool once target pseudo labels have been assigned by a DA algorithm. We can compute the gap  $\inf_{x \in \nu_1} g(x) - \sup_{x \in \nu_2} g(x)$  based on pseudo-labeled partition of the target distribution  $\nu_1$  and  $\nu_2$ . In addition to global assessment, the individual g(x) values can also serve as confidence indicators. Specifically, for target samples pseudo-labeled as class  $\nu_2$ , larger g(x) values indicate higher classification confidence; conversely, for samples labeled as class  $\nu_1$ , smaller g(x) values indicate higher confidence.

**Remark 3.** Although a similar version of Theorem 6 can be derived in the discrete OT setting using analogous techniques, we choose to adopt the semi-discrete OT formulation for computing the OT score in our work, due to the following reasons:

- (1) Improved computational efficiency: Semi-discrete OT offers better computational complexity compared to fully discrete OT.
- (2) Efficient incremental optimization: When a subset of data points is added or removed, the optimization of semi-discrete OT can be efficiently continued using stochastic gradient descent (SGD), without requiring a full recomputation from scratch.
- (3) Handling ambiguity in low-confidence filtering: In the discrete case, there exists ambiguity in determining which points should be eliminated as low-confidence samples—whether to remove

points with split weights across transport plans, or those with only small transport margins. The semi-discrete formulation mitigates such ambiguity by providing more stable and geometrically meaningful transport behavior.

The following corollary might be helpful in some computation scenarios.

**Corollary 7.** Under assumptions of 6 and suppose m and l are the weight vectors associated with  $T_{\nu_1}^{\hat{\mu}_1}$  and  $T_{\nu_2}^{\hat{\mu}_2}$ , respectively. Then  $(T_{\nu}^{\hat{\mu}})_{\#}\nu_1 = \hat{\mu}_1$  and  $(T_{\nu}^{\hat{\mu}})_{\#}\nu_2 = \hat{\mu}_2$  if and only if

$$\sup_{x\in\nu_1} \max_{z\in\hat{\mu}_2} \min_{y\in\hat{\mu}_1} \tilde{d}_{\boldsymbol{m}}(x,y) - \tilde{d}_{\boldsymbol{l}}(x,z) \leq \inf_{x\in\nu_2} \max_{z\in\hat{\mu}_2} \min_{y\in\hat{\mu}_1} \tilde{d}_{\boldsymbol{m}}(x,y) - \tilde{d}_{\boldsymbol{l}}(x,z).$$

### 5 OT score Computation

In this section, we present the algorithm used to compute the OT score and extend the definition to multiclass setting. Specifically, we model the source distribution in the feature space as a discrete measure and treat the target data as samples drawn from a continuous measure. Our approach is developed under the few-shot Source-Free UDA setting, where only very limited source information of feature representations is available. In the experimental section, we demonstrate that the OT score achieves strong performance even when using only the class-wise mean feature representations from the source domain. This not only reduces the computational complexity but also addresses privacy and security concerns associated with access to full source data.

**Definition 1.** Suppose the source data (or features)  $X^S$  consists of c classes. For each target sample x with pseudo label i and any class label j, we define the binary OT score as

$$g_j(x) := \max_{y \in \mathbf{X}^{S_i}} \min_{z \in \mathbf{X}^{S_j}} \tilde{d}(x, z) - \tilde{d}(x, y),$$

where  $\tilde{d}(\cdot,\cdot)$  requires computing the semi-discrete OT. And we define the OT score on target samples as

$$g(x) := \min_{j} g_{j}(x).$$

We summarize our OT score computation in Algorithm 1.

#### Algorithm 1 OT score

- 1: **Input:** Source feature representations  $\mathbf{Z}^{\mathcal{S}}$ , corresponding labels  $y^{\mathcal{S}}$ , source sample weights a, target features  $\mathbf{Z}^{\mathcal{T}}$  and corresponding predicted labels (or pseudo labels)  $\hat{y}^{\mathcal{T}}$ , entropic regularization parameter  $\varepsilon$ , learning rate  $\gamma$ .
- 2: Initialize  $w_0 = 0$ .
- 3: Compute class proportions  $p_c = \frac{|\{z_i^T \in \mathbf{Z}^T : \hat{y}_i^T = c\}|}{|\hat{y}^T|}$ .
- 4: **for**  $t = 1, 2, ..., max\_iter$  **do**
- 5: Draw a batch of samples  $\mathbf{Z}_{B_t}^{\mathcal{T}}$  from  $\mathbf{Z}^{\mathcal{T}}$ .
- 6: Compute smoothed indicator functions of Laguerre cells  $\mathbb{L}_{w_t}(z_i^{\mathcal{S}})$  for each  $z_i^{\mathcal{S}}$ :

$$\chi_j^{\varepsilon}(x, \boldsymbol{w}) = \frac{e^{\frac{-\|x - z_j^{\varepsilon}\| + \boldsymbol{w}_t^j}{\varepsilon}}}{\sum_{\ell} e^{\frac{-\|x - z_\ell^{\varepsilon}\| + \boldsymbol{w}_t^j}{\varepsilon}}}.$$

- 7: Update  $w_t$ :  $w_{t+1} = w_t \gamma \left[ \chi_j^{\varepsilon}(x, w_t) a_j \right]_{j=1}^{N_S} \in \mathbb{R}^{N_S}$ .
- 8: end for
- 9: for  $(z_i^{\mathcal{T}}, \hat{\pmb{y}}_i^{\mathcal{T}}) \in (\mathbf{Z}^{\mathcal{T}}, \hat{\pmb{y}}^{\mathcal{T}})$  do
- 10: Compute  $g_j(x) := \max_{y \in \mathbf{X}_{\tilde{y}_i^T}} \min_{z \in \mathbf{X}_j} \tilde{d}(x, z) \tilde{d}(x, y)$  for each class j.
- 11: Compute OT score of  $z_i^T$ :  $g(z_i^T) = \min_i g_i(z_i^T)$
- **12: end for**

**Remark 4.** Inspired by the OT score, we propose SDOT-DA, a simple yet effective algorithm for UDA. It assigns labels to targets based on the semi-discrete OT map from target features to source features, using the labels of their transport destinations. Further details are provided in Appendix C.

### 6 Experiemnts

In this section, we present experiments to evaluate the effectiveness of our algorithms. Additional details and results are provided in Appendix D.

#### 6.1 Synthetic Data

In this section, we use synthetic data to validate and illustrate our theoretical findings. Specifically, we consider a 2D scenario where data points are sampled from circular regions. The source domain consists of class-separated samples drawn from disjoint circles, whereas the target domain includes clusters with partial overlap. The distribution of the generated data is visualized in Figure 2(a). We compute the max-min values as described in Theorem 6 and present the results in Figure 2(b). As shown in Figure 2(c), the SDOTDA algorithm produces label predictions in which many samples within the overlapping regions are misclassified. However, after removing low-confidence predictions, the remaining samples are almost entirely classified correctly, as illustrated in Figure 2(d). Notably, the separation between the two clusters becomes significantly more obvious after this filtering step. Additional binary digit classification results under added noise conditions are provided in Appendix D.

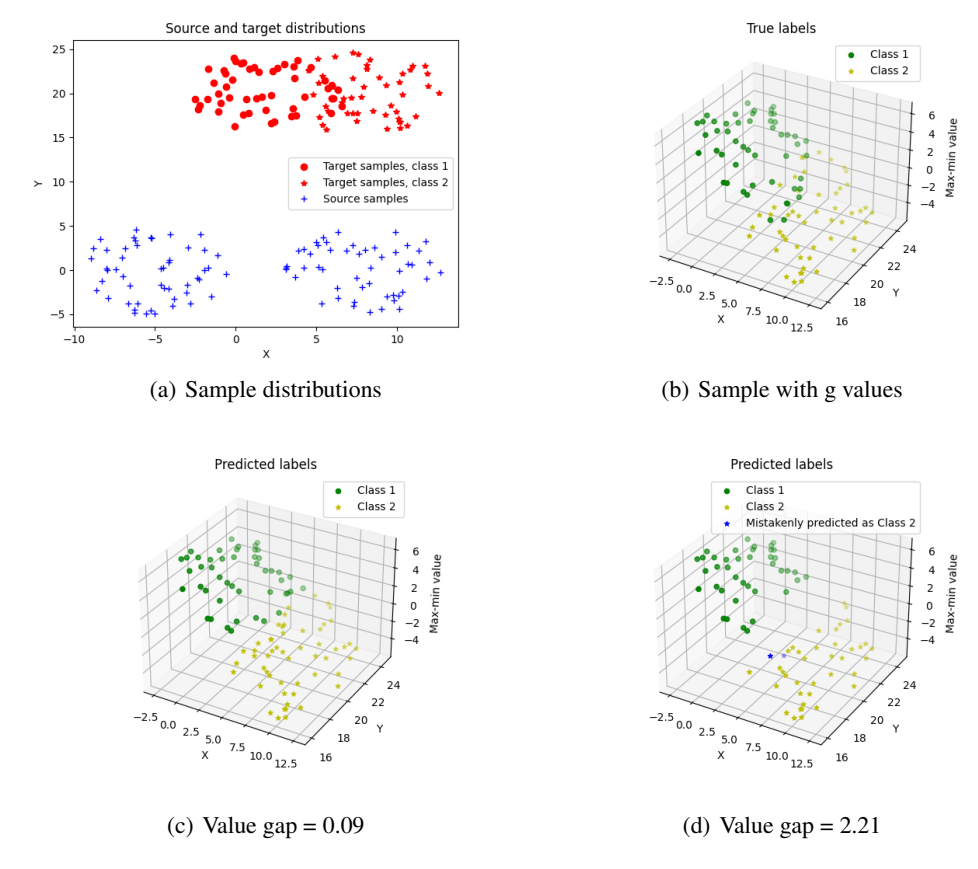


Figure 2: OT score performance on overlapping distributions.

### 6.2 Real World Datasets

To demonstrate the effectiveness of the proposed OT score, we compare it against several widely-used confidence estimation methods, including Maxprob, Entropy (Ent), and JMDS. The evaluation is conducted on four standard UDA benchmarks: Digits, Office-Home, ImageCLEF-DA, and VisDA-17. We compute confidence scores in the feature space extracted by the last layer of our neural network.

For evaluation, we adopt the Area Under the Risk-Coverage Curve (AURC) proposed by [7] [5] and subsequently employed in [15]. Specifically, after obtaining the high-confidence subset  $X_h^{\mathcal{T}}$ :

Table 2: Evaluation of confidence scores based on AURC (GMM).

Dataset	Task	Maxprob	Ent	Cossim	JMDS	OT Score
	$\mathbf{M} \to \mathbf{U}$	0.0055	0.0049	0.0051	0.0053	0.0033
Digits	$\boldsymbol{U} \to \boldsymbol{M}$	0.0224	0.0228	0.0204	0.0355	0.0214
	Avg.	0.0140	0.0139	0.0128	0.0204	0.0124
	$Ar \rightarrow Cl$	0.2823	0.2860	0.2871	0.2825	0.2777
	$\text{Ar} \rightarrow \text{Pr}$	0.1320	0.1353	0.1219	0.1328	0.1313
	$\text{Ar} \rightarrow \text{Rw}$	0.0782	0.0835	0.1073	0.0820	0.0810
	$Cl \rightarrow Ar$	0.2421	0.2450	0.2503	0.2971	0.2218
	$Cl \rightarrow Pr$	0.1489	0.1517	0.1336	0.1708	0.1354
Office-Home	$Cl \rightarrow Rw$	0.1366	0.1384	0.1412	0.1595	0.1241
Office-Hoffie	$\text{Pr} \rightarrow \text{Ar}$	0.2355	0.2453	0.2580	0.2715	0.2425
	$\text{Pr} \to \text{Cl}$	0.3417	0.3419	0.3180	0.3390	0.3257
	$\text{Pr} \rightarrow \text{Rw}$	0.0836	0.0875	0.1007	0.0952	0.0781
	$Rw \to Ar$	0.1439	0.1487	0.1785	0.1750	0.1391
	$Rw \to Cl$	0.2826	0.2812	0.2762	0.2760	0.2613
	$Rw \to Pr$	0.0693	0.0713	0.0725	0.0890	0.0637
	Avg.	0.1814	0.1846	0.1871	0.1971	0.1735
VisDA-2017	$T \to V$	0.3327	0.3312	0.3494	0.3090	0.2916

 $\left\{x_i^{\mathcal{T}} \mid s\left(x_i^{\mathcal{T}}, \hat{y}_i^{\mathcal{T}}\right) > h\right\}$ , where h is a predefined confidence threshold, the risk is computed as the average empirical loss over  $X_h^{\mathcal{T}}$ , and the coverage corresponds to  $\left|X_h^{\mathcal{T}}\right| / \left|X^{\mathcal{T}}\right|$ . A lower AURC value indicates higher confidence reliability, as it implies a lower prediction risk at a given coverage level. Notably, when the 0/1 loss is applied, a high AURC reflects a high error rate among pseudo-labels, thus indicating poor correctness and calibration of the confidence scores.

To further assess the robustness of the proposed OT score under varying pseudo-label quality, we consider two evaluation scenarios: (1) pseudo labels obtained using a Gaussian Mixture Model (GMM); and (2) pseudo labels generated by the DSAN algorithm [32] with 20 epochs of training.

Under setting (1), Maxprob and Ent uses labels assigned by the pretrained source classifier while Cossim, JMDS, OT score receive pseudo labels from a Gaussian Mixture Model (GMM). We also considered to assign pseudo labels using the SDOT-DA algorithm. However, empirical results showed that GMM-based labels yield better performance. Therefore, for the comparisons presented in Table 2, we adopt GMM-generated pseudo labels for computing the OT score. Under setting (2), only Cossim and OT score are capable of incorporating externally generated high-quality pseudo labels. We continue under the setting where only the mean feature representation of each source class is available. Table 1 shows the significant benefits of leveraging high quality pseudo labels. The OT score achieved the lowest AURC value in most adaptation tasks across the considered scenarios.

### 7 Conclusion and Future Work

We investigate theoretical guarantees about allowed distribution shifts in order to have a label-preserving OT. Using semi-discrete OT, we derive the OT score which considers the decision boundary induced by the OT alignment. The definition of OT score can be easily extended to other cost functions other than the standard Euclidean norm. Additionally, confidence scores are helpful for sample reweighting during training process. Since optimization of semi-discrete OT can be efficiently continued using stochastic gradient descent (SGD), it is also useful to propose a recomputation scheme for OT score during training.

Also, in our experiments, we only use the source mean class features for the discrete measure, it remains to explore how to increase the source information in the most efficient way. Intuitively, we want to replace the source empirical distribution  $\hat{\mu}$  by  $\hat{\mu}_{new}$  defined on a smaller finite set such that  $T^{\hat{\mu}}_{\nu} \approx T^{\hat{\mu}_{new}}_{\nu}$ . We leave this investigation for future work.

### References

- [1] Shai Ben-David and Ruth Urner. On the hardness of domain adaptation and the utility of unlabeled target samples. In *International Conference on Algorithmic Learning Theory*, pages 139–153. Springer, 2012.
- [2] Yann Brenier. Polar factorization and monotone rearrangement of vector-valued functions. *Communications on pure and applied mathematics*, 44(4):375–417, 1991.
- [3] Nicolas Courty, Rémi Flamary, Devis Tuia, and Alain Rakotomamonjy. Optimal transport for domain adaptation. *IEEE transactions on pattern analysis and machine intelligence*, 39(9): 1853–1865, 2016.
- [4] Bharath Bhushan Damodaran, Benjamin Kellenberger, Rémi Flamary, Devis Tuia, and Nicolas Courty. Deepjdot: Deep joint distribution optimal transport for unsupervised domain adaptation. In *Proceedings of the European conference on computer vision (ECCV)*, pages 447–463, 2018.
- [5] Yukun Ding, Jinglan Liu, Jinjun Xiong, and Yiyu Shi. Revisiting the evaluation of uncertainty estimation and its application to explore model complexity-uncertainty trade-off. In *Proceedings* of the IEEE/CVF Conference on Computer Vision and Pattern Recognition Workshops, pages 4–5, 2020.
- [6] Yonatan Geifman and Ran El-Yaniv. Selective classification for deep neural networks. *Advances in neural information processing systems*, 30, 2017.
- [7] Yonatan Geifman, Guy Uziel, and Ran El-Yaniv. Bias-reduced uncertainty estimation for deep neural classifiers. *arXiv preprint arXiv:1805.08206*, 2018.
- [8] Darius Geiß, Rolf Klein, Rainer Penninger, and Günter Rote. Optimally solving a transportation problem using voronoi diagrams. *Computational Geometry*, 46(8):1009–1016, 2013.
- [9] Xavier Glorot, Antoine Bordes, and Yoshua Bengio. Domain adaptation for large-scale sentiment classification: A deep learning approach. In *Proceedings of the 28th international conference on machine learning (ICML-11)*, pages 513–520, 2011.
- [10] Valentin Hartmann and Dominic Schuhmacher. Semi-discrete optimal transport-the case p= 1. *arXiv preprint arXiv:1706.07650*, 2017.
- [11] Wenlong Ji, Yiping Lu, Yiliang Zhang, Zhun Deng, and Weijie J Su. An unconstrained layer-peeled perspective on neural collapse. *arXiv preprint arXiv:2110.02796*, 2021.
- [12] Vignesh Kothapalli. Neural collapse: A review on modelling principles and generalization. *arXiv preprint arXiv:2206.04041*, 2022.
- [13] Balaji Lakshminarayanan, Alexander Pritzel, and Charles Blundell. Simple and scalable predictive uncertainty estimation using deep ensembles. *Advances in neural information processing systems*, 30, 2017.
- [14] Trung Le, Tuan Nguyen, Nhat Ho, Hung Bui, and Dinh Phung. Lamda: Label matching deep domain adaptation. In *International Conference on Machine Learning*, pages 6043–6054. PMLR, 2021.
- [15] Jonghyun Lee, Dahuin Jung, Junho Yim, and Sungroh Yoon. Confidence score for source-free unsupervised domain adaptation. In *International conference on machine learning*, pages 12365–12377. PMLR, 2022.
- [16] Mingsheng Long, Yue Cao, Jianmin Wang, and Michael Jordan. Learning transferable features with deep adaptation networks. In *International conference on machine learning*, pages 97–105. PMLR, 2015.
- [17] Mingsheng Long, Han Zhu, Jianmin Wang, and Michael I Jordan. Deep transfer learning with joint adaptation networks. In *International conference on machine learning*, pages 2208–2217. PMLR, 2017.

- [18] Jianfeng Lu and Stefan Steinerberger. Neural collapse under cross-entropy loss. *Applied and Computational Harmonic Analysis*, 59:224–241, 2022.
- [19] Amit Mandelbaum and Daphna Weinshall. Distance-based confidence score for neural network classifiers. *arXiv preprint arXiv:1709.09844*, 2017.
- [20] Tanya Nair, Doina Precup, Douglas L Arnold, and Tal Arbel. Exploring uncertainty measures in deep networks for multiple sclerosis lesion detection and segmentation. *Medical image analysis*, 59:101557, 2020.
- [21] Vardan Papyan, XY Han, and David L Donoho. Prevalence of neural collapse during the terminal phase of deep learning training. *Proceedings of the National Academy of Sciences*, 117 (40):24652–24663, 2020.
- [22] Gabriel Peyré, Marco Cuturi, et al. Computational optimal transport: With applications to data science. *Foundations and Trends*® *in Machine Learning*, 11(5-6):355–607, 2019.
- [23] Ievgen Redko, Amaury Habrard, and Marc Sebban. Theoretical analysis of domain adaptation with optimal transport. In *Machine Learning and Knowledge Discovery in Databases: European Conference, ECML PKDD 2017, Skopje, Macedonia, September 18–22, 2017, Proceedings, Part II 10*, pages 737–753. Springer, 2017.
- [24] Ievgen Redko, Amaury Habrard, and Marc Sebban. On the analysis of adaptability in multisource domain adaptation. *Machine Learning*, 108(8):1635–1652, 2019.
- [25] Mohammad Rostami and Aram Galstyan. Overcoming concept shift in domain-aware settings through consolidated internal distributions. In *Proceedings of the AAAI conference on artificial intelligence*, volume 37, pages 9623–9631, 2023.
- [26] Filippo Santambrogio. Optimal transport for applied mathematicians. *Birkäuser*, *NY*, 55(58-63): 94, 2015.
- [27] Mariia Seleznova, Dana Weitzner, Raja Giryes, Gitta Kutyniok, and Hung-Hsu Chou. Neural (tangent kernel) collapse. *Advances in Neural Information Processing Systems*, 36, 2024.
- [28] Tom Tirer and Joan Bruna. Extended unconstrained features model for exploring deep neural collapse. In *International Conference on Machine Learning*, pages 21478–21505. PMLR, 2022.
- [29] Alexey Tsymbal. The problem of concept drift: definitions and related work. *Computer Science Department, Trinity College Dublin*, 106, 2004.
- [30] Cédric Villani et al. Optimal transport: old and new, volume 338. Springer, 2009.
- [31] Jiayao Zhang, Hua Wang, and Weijie Su. Imitating deep learning dynamics via locally elastic stochastic differential equations. *Advances in Neural Information Processing Systems*, 34: 6392–6403, 2021.
- [32] Yongchun Zhu, Fuzhen Zhuang, Jindong Wang, Guolin Ke, Jingwu Chen, Jiang Bian, Hui Xiong, and Qing He. Deep subdomain adaptation network for image classification. *IEEE transactions on neural networks and learning systems*, 32(4):1713–1722, 2020.

### A Confidence Scores

We provide details of the confidence scores used for comparison. Let  $x_i^{\mathcal{T}}$  denote the i-th target sample, and let  $p_{\mathcal{S}}$  represent the class probability predicted by the pretrained source model. Here, K is the total number of classes, and  $C_{\hat{y}_i^{\mathcal{T}}}$  denotes the center of the cluster corresponding to the predicted label  $\hat{y}_i^{\mathcal{T}}$  for  $x_i^{\mathcal{T}}$ .

$$\operatorname{Maxprob}\left(x_{i}^{\mathcal{T}}\right) = \max_{c} p_{\mathcal{S}}\left(x_{i}^{\mathcal{T}}\right)_{c},$$

$$\operatorname{Ent}\left(x_{i}^{\mathcal{T}}\right) = 1 + \frac{\sum_{c=1}^{K} p_{\mathcal{S}}\left(x_{i}^{\mathcal{T}}\right)_{c} \log p_{\mathcal{S}}\left(x_{i}^{\mathcal{T}}\right)_{c}}{\log K},$$

$$\operatorname{Cossim}\left(x_{i}^{\mathcal{T}}\right) = \frac{1}{2}\left(1 + \frac{\left\langle x_{i}^{\mathcal{T}}, C_{\hat{y}_{i}^{\mathcal{T}}} \right\rangle}{\left\|x_{i}^{\mathcal{T}}\right\| \left\|C_{\hat{y}_{i}^{\mathcal{T}}}\right\|}\right).$$

JMDS score is computed by JMDS  $\left(x_i^{\mathcal{T}}\right) = \mathrm{LPG}\left(x_i^{\mathcal{T}}\right) \cdot \mathrm{MPPL}\left(x_i^{\mathcal{T}}\right)$ . LPG is the Log-Probability Gap computed from log data-structure-wise probability  $\log p_{\mathrm{data}}\left(x_i^{\mathcal{T}}\right)$  using GMM on the target feature space. MPPL provides high scores for samples whose GMM pseudo-label is the same based on  $p_{\mathcal{S}}\left(x_i^{\mathcal{T}}\right)$  and  $p_{\mathrm{data}}\left(x_i^{\mathcal{T}}\right)$ . Details about JMDS score can be found in [15].

### **B** Proofs

*Proof of Theorem 4.* Due to the concentration assumptions on  $\mu$  and  $\nu$ , we can pick sets  $E_{\mu_i}$  and  $E_{\nu_i}$  such that  $\mu_1(E_{\mu_1}) = \mu_2(E_{\mu_2}) \geq 1 - \epsilon$ . So  $\frac{1}{2} + \frac{1}{2}\epsilon \geq \mu(E_{\mu_i}) \geq \frac{1}{2} - \frac{1}{2}\epsilon$ . The same holds for  $\nu(E_{\nu_i})$ .

Consider  $F_i = (T^{\mu}_{\nu})^{-1}(E_{\mu_i})$ , we have  $\nu(F_i) = \mu(E_{\mu_i}) \ge \frac{1}{2} - \frac{1}{2}\epsilon$  as well. Let  $F = F_1 \cup F_2$ . So  $E_{\nu_i} \cap F$  is a bounded set with

$$\frac{1}{2} + \frac{1}{2}\epsilon \ge \nu(E_{\nu_i} \cap F) = \nu(E_{\nu_i}) - \nu(E_{\nu_i} \cap F^c) \tag{1}$$

$$\geq \frac{1}{2} - \frac{1}{2}\epsilon - \nu(F^c) \tag{2}$$

$$\geq \frac{1}{2} - \frac{1}{2}\epsilon - \epsilon = \frac{1}{2} - \frac{3}{2}\epsilon \tag{3}$$

Without loss of generality, we assume  $\nu(E_{\nu_1} \cap F) \ge \nu(E_{\nu_2} \cap F)$ . Since  $\nu \ll \mathcal{L}$ , we can pick R > 0 such that  $\nu(E_{\nu_1} \cap F \cap B_R) = \nu(E_{\nu_2} \cap F)$ .

Now consider the optimal transport map  $T^{\mu}_{\nu}$  restricted on  $(E_{\nu_1} \cap F \cap B_R) \cup (E_{\nu_2} \cap F)$ . By [30, Theorem 4.6], this restricted map is an optimal transport map between the marginal measures.

Since  $\mu(T^{\mu}_{\nu}(E_{\nu_1}\cap F\cap B_R)\cup T^{\mu}_{\nu}(E_{\nu_2}\cap F))=\nu((E_{\nu_1}\cap F\cap B_R)\cup (E_{\nu_2}\cap F))\geq 1-3\epsilon$ , we get an estimate  $\mu((T^{\mu}_{\nu}(E_{\nu_1}\cap F\cap B_R)\cup T^{\mu}_{\nu}(E_{\nu_2}\cap F))\cap E_{\mu_i})\geq (1-3\epsilon)-(\frac{1}{2}+\frac{1}{2}\epsilon)=\frac{1}{2}-\frac{7}{2}\epsilon$ . Therefore, we can use Lemma 8 to conclude that with probability greater than  $1-7\epsilon$ , target samples will be correctly classified after optimal transportation.

**Lemma 8.** Suppose we have probability measures  $\mu_i$  and  $\nu_i$  with bounded support. Also assume that  $\operatorname{supp} \mu_1$  and  $\operatorname{supp} \mu_2$  are disjoint,  $\operatorname{supp} \nu_1$  and  $\operatorname{supp} \nu_2$  are disjoint. Let  $r_{\mu_i}$  denote the diameter of the support of  $\mu_i$  and set  $l_i = d(\operatorname{supp} \mu_i, \operatorname{supp} \nu_i)$ ,  $L_1 = d(\operatorname{supp} \mu_1, \operatorname{supp} \nu_2)$ ,  $L_2 = d(\operatorname{supp} \mu_2, \operatorname{supp} \nu_1)$ . Suppose  $\mu := \frac{1}{2}\mu_1 + \frac{1}{2}\mu_2$ ,  $\nu := p\nu_1 + (1-p)\nu_2$  for some  $p \in (0, \frac{1}{2}]$ . If  $(r_{\mu_1} + r_{\nu_1} + l_1) + (r_{\mu_2} + r_{\nu_2} + l_2) < L_1 + L_2$ , then  $T^{\mu}_{\nu}(\operatorname{supp} \nu_1) \subset \operatorname{supp} \mu_1$  up to a negligible set.

Proof of Lemma 8. Suppose there exists a set  $A \subset \operatorname{supp} \nu_1$  with  $\nu(A) = \delta > 0$  and  $T^{\mu}_{\nu}(A) \subset \operatorname{supp} \mu_2$ . Then there must be a set  $B \subset \operatorname{supp} \nu_2$  with  $\nu(B) \geq \delta + 1 - p - \frac{1}{2} = \frac{1}{2} + \delta - p$  and  $T^{\mu}_{\nu}(B) \subset \operatorname{supp} \mu_1$ . Since  $\nu_i \ll \mathcal{L}$ , we can pick  $B' \subset B$  such that  $\nu(B') = \delta$ . Then for any

measurable  $\tilde{T}$  such that  $\tilde{T}(A) = T^{\mu}_{\nu}(B')$  and  $\tilde{T}(B') = T^{\mu}_{\nu}(A)$ ,

$$\int_{A \cup B'} \|\tilde{T}(x) - x\| \ dx \le \delta(r_{\mu_1} + r_{\nu_1} + l_1) + \delta(r_{\mu_2} + r_{\nu_2} + l_2) < \delta(L_1 + L_2) \le \int_{A \cup B'} \|T^{\mu}_{\nu}(x) - x\| \ dx,$$

which contradicts the optimality of  $T^{\mu}_{\nu}$ .

*Proof of Theorem 6.* Let w be any weight vector associated with  $T_{\bar{\nu}}^{\hat{\mu}}$ . We start with the observation that  $(T_{\bar{\nu}}^{\hat{\mu}})_{\#}\bar{\nu}_{1}=\hat{\mu}_{1}$  and  $(T_{\bar{\nu}}^{\hat{\mu}})_{\#}\bar{\nu}_{2}=\hat{\mu}_{2}$  is equivalent to the following two conditions:

- (1) For  $\forall x \in \bar{\nu}_1, \tilde{d}_{\boldsymbol{w}}(x, \hat{\mu}_1) \leq \tilde{d}_{\boldsymbol{w}}(x, \hat{\mu}_2).$
- (2) And for  $\forall x \in \bar{\nu}_2$ ,  $\tilde{d}_{\boldsymbol{w}}(x, \hat{\mu}_2) \leq \tilde{d}_{\boldsymbol{w}}(x, \hat{\mu}_1)$ .
- (1) requires any point from  $\bar{\nu}_1$  to be assigned to some point in  $\hat{\mu}_1$  and (2) requires any point from  $\bar{\nu}_2$  to be assigned to some point in  $\hat{\mu}_2$ , i.e.

$$\sup_{x \in \bar{\nu_1}} \tilde{d}_{\boldsymbol{w}}(x, \hat{\mu}_1) - \tilde{d}_{\boldsymbol{w}}(x, \hat{\mu}_2) \le 0 \le \inf_{x \in \bar{\nu_2}} \tilde{d}_{\boldsymbol{w}}(x, \hat{\mu}_1) - \tilde{d}_{\boldsymbol{w}}(x, \hat{\mu}_2). \tag{4}$$

We rewrite 4 by unwarpping the definition of  $\tilde{d}$  to get

$$\sup_{x \in \bar{\nu_1}} \left( \min_{y \in \hat{\mu}_1} \tilde{d}_{\boldsymbol{w}}(x,y) \right) - \left( \min_{z \in \hat{\mu}_2} \tilde{d}_{\boldsymbol{w}}(x,z) \right) \leq 0 \leq \inf_{x \in \bar{\nu_2}} \left( \min_{y \in \hat{\mu}_1} \tilde{d}_{\boldsymbol{w}}(x,y) \right) - \left( \min_{z \in \hat{\mu}_2} \tilde{d}_{\boldsymbol{w}}(x,z) \right), \tag{5}$$

i.e.

$$\sup_{x \in \bar{\nu}_1} \max_{z \in \hat{\mu}_2} \min_{y \in \hat{\mu}_1} \tilde{d}_{\boldsymbol{w}}(x, y) - \tilde{d}_{\boldsymbol{w}}(x, z) \le 0 \le \inf_{x \in \bar{\nu}_2} \max_{z \in \hat{\mu}_2} \min_{y \in \hat{\mu}_1} \tilde{d}_{\boldsymbol{w}}(x, y) - \tilde{d}_{\boldsymbol{w}}(x, z). \tag{6}$$

Proof of Corollary 7. Observe that  $w_1 = m + C$  and  $w_2 = l + D$  are also weight vectors for  $T_{\bar{\nu}_1}^{\hat{\mu}_1}$  and  $T_{\bar{\nu}_2}^{\hat{\mu}_2}$  for any constants C and D.

Moreover,

$$\sup_{x\in\bar{\nu_1}} \max_{z\in\hat{\mu}_2} \min_{y\in\hat{\mu}_1} \tilde{d}_{\boldsymbol{w}_1}(x,y) - \tilde{d}_{\boldsymbol{w}_2}(x,z) \leq \inf_{x\in\bar{\nu}_2} \max_{z\in\hat{\mu}_2} \min_{y\in\hat{\mu}_1} \tilde{d}_{\boldsymbol{w}_1}(x,y) - \tilde{d}_{\boldsymbol{w}_2}(x,z),$$

which is the same as

$$C - D + \sup_{x \in \bar{\nu}_1} \max_{z \in \hat{\mu}_2} \min_{y \in \hat{\mu}_1} \tilde{d}_{\boldsymbol{m}}(x, y) - \tilde{d}_{\boldsymbol{l}}(x, z) \le C - D + \inf_{x \in \bar{\nu}_2} \max_{z \in \hat{\mu}_2} \min_{y \in \hat{\mu}_1} \tilde{d}_{\boldsymbol{m}}(x, y) - \tilde{d}_{\boldsymbol{l}}(x, z).$$
(7)

Choosing the difference C-D allows us to conclude  $(T_{\bar{\nu}}^{\hat{\mu}})_{\#}\bar{\nu}_1=\hat{\mu}_1$  and  $(T_{\bar{\nu}}^{\hat{\mu}})_{\#}\bar{\nu}_2=\hat{\mu}_2$  by setting  $\boldsymbol{w}=[\boldsymbol{w}_1,\boldsymbol{w}_2].$ 

Conversely, let  ${\boldsymbol w}$  be the corresponding weight vector of  $T^{\hat{\mu}}_{\bar{\nu}}$  and assume  $(T^{\hat{\mu}}_{\bar{\nu}})_{\#}\bar{\nu}_1=\hat{\mu}_1, (T^{\hat{\mu}}_{\bar{\nu}})_{\#}\bar{\nu}_2=\hat{\mu}_2$ . Then  ${\boldsymbol w}_1$  (or  ${\boldsymbol w}_2$ ) differs from  ${\boldsymbol m}$  (or  ${\boldsymbol l}$ ) by some constant C (or D) [8, Theorem 2]. By Theorem 6,

$$\sup_{x \in \bar{\nu_1}} \max_{z \in \hat{\mu}_2} \min_{y \in \hat{\mu}_1} \tilde{d}_{w_1}(x, y) - \tilde{d}_{w_2}(x, z) \le 0 \le \inf_{x \in \bar{\nu}_2} \max_{z \in \hat{\mu}_2} \min_{y \in \hat{\mu}_1} \tilde{d}_{w_1}(x, y) - \tilde{d}_{w_2}(x, z),$$

which implies

$$C - D + \sup_{x \in \bar{\nu}_1} \max_{z \in \hat{\mu}_2} \min_{y \in \hat{\mu}_1} \tilde{d}_{\boldsymbol{m}}(x, y) - \tilde{d}_{\boldsymbol{l}}(x, z) \le 0 \le C - D + \inf_{x \in \bar{\nu}_2} \max_{z \in \hat{\mu}_2} \min_{y \in \hat{\mu}_1} \tilde{d}_{\boldsymbol{m}}(x, y) - \tilde{d}_{\boldsymbol{l}}(x, z),$$

i.e.

$$\sup_{x\in\bar{\nu_1}} \max_{z\in\hat{\mu}_2} \min_{y\in\hat{\mu}_1} \tilde{d}_{\boldsymbol{m}}(x,y) - \tilde{d}_{\boldsymbol{l}}(x,z) \leq D - C \leq \inf_{x\in\bar{\nu_2}} \max_{z\in\hat{\mu}_2} \min_{y\in\hat{\mu}_1} \tilde{d}_{\boldsymbol{m}}(x,y) - \tilde{d}_{\boldsymbol{l}}(x,z).$$

### C SDOTDA

#### C.1 Semi-discrete OT for Domain Adaptation

We treat the source distribution as a discrete probability measure and the target distribution as a continuous probability measure that is absolutely continuous with respect to the Lebesgue measure. SDOT-DA assigns labels to target samples based on the semi-discrete OT map from target features to source features, using the labels of their transport destinations.

### **Algorithm 2 SDOTDA**

- 1: **Input:** Pre-trained model  $f_{\theta} = h_{\boldsymbol{w}} \circ \phi_{\boldsymbol{v}}$ , discrete probability measure  $\hat{\mu}$  constructed from  $N_{\mathcal{S}}$  source feature samples  $\phi_{\boldsymbol{v}}(\mathbf{X}_{\mathcal{S}})$ , source data labels  $\mathbf{Y}_{\mathcal{S}}$ , target data samples  $\mathbf{X}_{\mathcal{T}}$ , entropic regularization parameter  $\varepsilon$ , learning rate  $\gamma$ .
- 2: Compute target features  $\nu := (\phi_{\boldsymbol{v}})_{\#} \nu_{\mathcal{T}}$ .
- 3: **for**  $iteration = 1, 2, ..., max\_iter$  **do**
- 4: Draw a sample x from  $\nu$ .
- 5: For each sample  $z_j \in \hat{\mu}$ , compute the smoothed version of the indicator function of the

Laguerre cell 
$$\mathbb{L}_{\boldsymbol{w}}(z_j)$$
:  $\chi_j^{\varepsilon}(x, \boldsymbol{w}) = \frac{e^{\frac{-\|x-z_j\|+w_j}{\varepsilon}}}{\sum_{\ell} e^{\frac{-\|x-z_\ell\|+w_j}{\varepsilon}}}.$ 

- 6: Update w with the stochastic gradient at x:  $w = w \gamma \left( \chi_j^{\varepsilon}(x, w) \frac{1}{N_S} \right)_{i=1}^{N_S} \in \mathbb{R}^{N_S}$ .
- 7: end for
- 8: for  $x \in \mathbf{X}_{\mathcal{T}}$  do
- 9: Compute  $j = \arg\max_{z_j \in \hat{\mu}} \chi_j^{\varepsilon}(x, \boldsymbol{w})$
- 10: Label of  $x \leftarrow$  label of  $z_i$
- 11: **end for**

**Remark 5.** An advantage of SDOTDA is that once the weight vector w is computed, we can easily classify new data points from the target distribution using the (approximated) indicator function without recomputing the semi-discrete OT. Also, this algorithm does not require to re-train the neural network so it is preferred when the target domain dataset is not sufficient for training a neural network.

As mentioned in section 4.2, we can use the weight vector  $\boldsymbol{w}$  obtained from algorithm 2 to compute the g values associated with each target data point as well as the g value gap between different classes, which allows us to filter out classified data with low confidence. Experimental results for algorithm 2 are demonstrated in Appendix D.2

When applying optimal transport to solve domain adaptation problems, usually we do not have any label information for the target dataset nor the number of data points in each class. Therefore, the class imbalance between distributions could limit the performance of optimal transport based algorithms. In order for the OT map to transport target data clusters to correct source data clusters, we may need to rescale the weights of sampling points from the source data so that the total class weights are the same across source and target distributions. Under neural collapse type assumptions, we can provide theoretical guarantees that this issue can be solved automatically by selecting the "optimal weights". We provide the theory and numerical validation with synthetic data in Appendix C.1.1.

#### C.1.1 Unbalance Classes

**Theorem 9.** With the same notations of 8, suppose  $\mu = p^*\mu_1 + (1-p^*)\mu_2$  for some  $p^* \in (0,1)$ . If  $L_i \ge l_i + r_{\nu_1} + r_{\nu_2} + r_{\mu_1} + r_{\mu_2}$  then  $\arg\min_{p \in [0,1]} W_1(\mu,\nu) = p^*$ , where  $\nu := p\nu_1 + (1-p)\nu_2$  for some  $p \in (0,1)$ .

*Proof.* W.L.O.G we assume  $p^*=\frac{1}{2}$ . Let T denote an OT map between  $\frac{1}{2}\nu_1+\frac{1}{2}\nu_2$  and  $\frac{1}{2}\mu_1+\frac{1}{2}\mu_2$ . Suppose  $\nu=(\frac{1}{2}+\delta)\nu_1+(\frac{1}{2}-\delta)\nu_2$ . Let  $F_1$  be the set such that  $F_1\subset\sup\nu_1$  and  $\nu_1(F_1)=\frac{2\delta}{1+2\delta}$  so that  $(\frac{1}{2}+\delta)\nu_1(F_1^C)=\frac{1}{2}$ . Let  $F_2\subset\sup\mu_2$  be defined as  $F_2:=T_{\nu}^{\mu}(F_1)$ . This can be done due

to Lemma 8. Given Lemma 8, it suffices to show the following inequality:

$$\int_{F_1} \|T_{\nu}^{\mu}(x) - x\| d((\frac{1}{2} + \delta)\nu_1) + \int_{F_1^C} \|T_{\nu}^{\mu}(x) - x\| d((\frac{1}{2} + \delta)\nu_1) + \int_{\text{supp }\nu_2} \|T_{\nu}^{\mu}(x) - x\| d((\frac{1}{2} - \delta)\nu_2) \\
\geq W_1(\frac{1}{2}\nu_1, \frac{1}{2}\mu_1) + W_1(\frac{1}{2}\nu_2, \frac{1}{2}\mu_2).$$

Denote  $\bar{\mu}_2 := (T^{\mu}_{\nu})_{\#}((\frac{1}{2} - \delta)\nu_2)$ . We can decompose  $W_1(\frac{1}{2}\nu_2, \frac{1}{2}\mu_2) = a + b$  where a corresponds to the cost on the source probability mass that forms  $\bar{\mu}_2$  and b corresponds to the cost on the rest of source probability mass. We denote the source marginal corresponding to a as  $\frac{1}{2}\tilde{\nu}_2$ . Then it remains to show

$$\int_{F_1} ||T_{\nu}^{\mu}(x) - x|| d((\frac{1}{2} + \delta)\nu_1) - b$$

$$\geq W_1(\frac{1}{2}\nu_1, \frac{1}{2}\mu_1) - \int_{F_1^C} ||T_{\nu}^{\mu}(x) - x|| d((\frac{1}{2} + \delta)\nu_1)$$

$$+ a - \int_{\text{supp }\nu_2} ||T_{\nu}^{\mu}(x) - x|| d((\frac{1}{2} - \delta)\nu_2)$$

Note  $\int_{F_1^C} \|T_{\nu}^{\mu}(x) - x\| d((\frac{1}{2} + \delta)\nu_1)$  achieves the optimal transport between  $(\frac{1}{2} + \delta)\nu_1$  restricted on  $F_1^C$  and  $\frac{1}{2}\mu_1$ . Also,  $\int_{\text{supp }\nu_2} \|T_{\nu}^{\mu}(x) - x\| d((\frac{1}{2} - \delta)\nu_2)$  achieves the optimal transport between  $(\frac{1}{2} - \delta)\nu_2$  and  $\bar{\mu}_2$ . By triangle inequality properties of  $W_1$  distance, it suffices to show

$$LHS \geq W_1(\frac{1}{2}\nu_1, (\frac{1}{2}+\delta)\nu_1|_{F_1^C}) + W_1(\frac{1}{2}\tilde{\nu}_2, (\frac{1}{2}-\delta)\nu_2).$$

Since

$$RHS < \delta r_{\nu_1} + \delta r_{\nu_2} < LHS$$

the optimality is proved.

We verify Theorem 9 with synthetic data generated within two circular clusters. We compute (discrete) OT plans under unbalanced cluster settings; see Figure 3 and Figure 4. In this experiment, we generate two equally sized clusters for the target samples, while the corresponding source clusters are assigned proportions of 0.2 and 0.8, respectively. As shown in the results, the optimal transport cost is minimized when the reweighting factor is correctly set to p=0.2. This observation supports our claim that optimizing the reweighting factor can effectively mitigate class imbalance in optimal transport—based domain adaptation. However, this finding has not yet been validated on real-world datasets, where the underlying distributions are significantly more complex. We leave this investigation for future work.

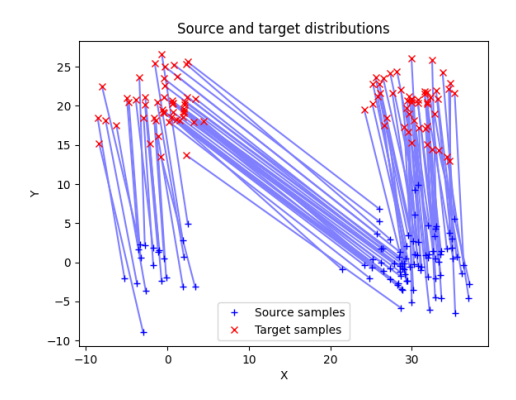


Figure 3: Unbalanced clusters with p=0.5

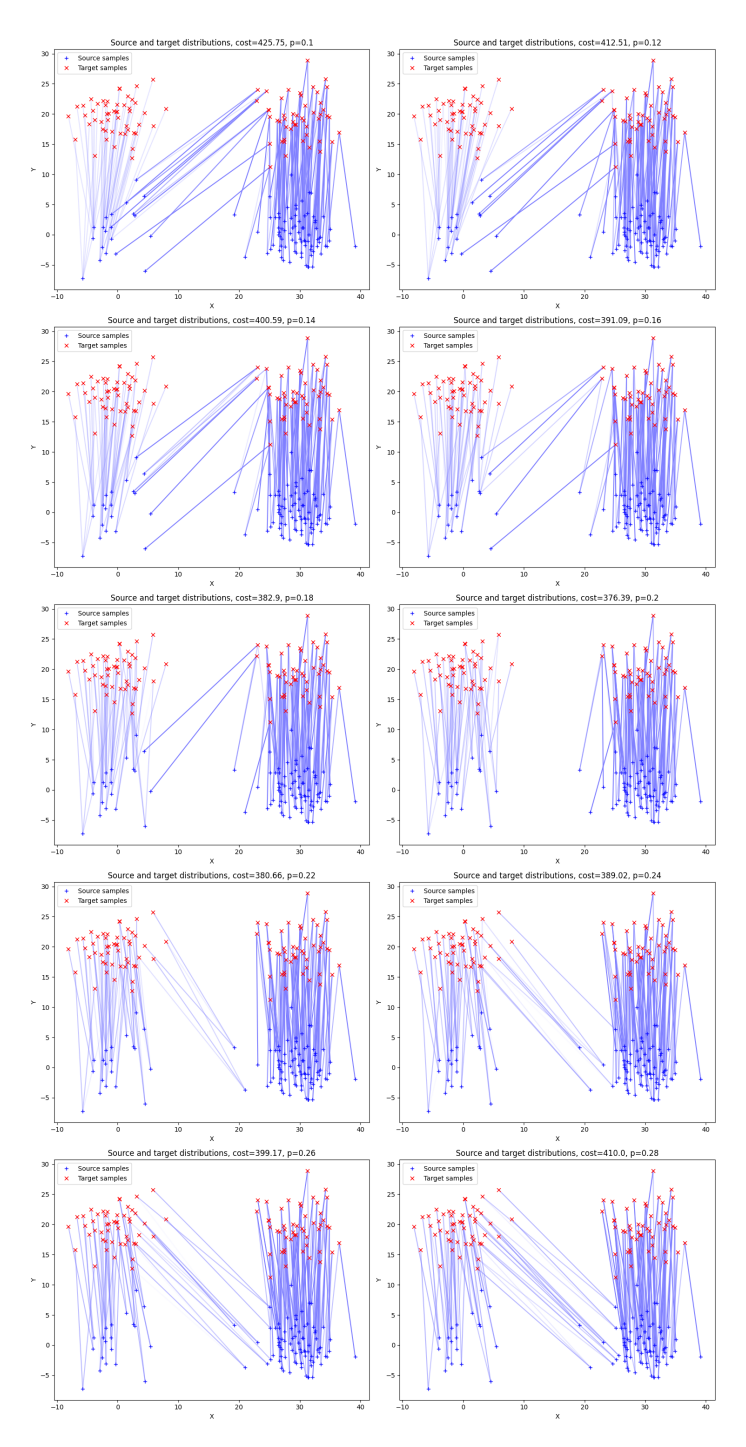


Figure 4: Unbalanced clusters

## D Experiment details

In our main experiments, we compare OT score with other confidence scores including Maxprob, Ent, Cossim, and JMDS. The details for other confidence scores are presented in Appendix A. We compare the performance of confidence scores on four standard UDA benchmarks: Digit recognition tasks, ImageCLEFDA, Office-Home, and VisDA-2017. All code can be efficiently executed on a single NVIDIA RTX 4070 GPU without requiring specialized hardware. For ImageCLEFDA, Office-Home, and VisDA-2017 datasets, we use ResNet-50 backbone pretrained on the ImageNet as a base network.

Then we finetune the pretrained network on source domain for 100 epochs. For the finetuning, We use SGD optimizer with the momentum term set to be 0.9. We set lr=1e-4 for the base network and lr=1e-3 for the classifier layer. For digit recognition tasks, we use the VGG16 network as the base model. The network is initialized with random weights. We finetune this network on source domains using lr=1e-4, epochs=50, momentum=0.9, decay=1e-4. For OT score computation, we set the entropic regularization parameter  $\varepsilon$  to be 0.5. A complete comparison for GMM pseudo labels is presented in Table 3.

Table 3: Evaluation of confidence scores based on AURC (GMM).

Dataset	Task	Maxprob	Ent	Cossim	JMDS	OT Score
	$\mathbf{M} \to \mathbf{U}$	0.0055	0.0049	0.0051	0.0053	0.0033
Digits	$\boldsymbol{U} \to \boldsymbol{M}$	0.0224	0.0228	0.0204	0.0355	0.0214
	Avg.	0.0140	0.0139	0.0128	0.0204	0.0124
	$\mathrm{C}  o \mathrm{I}$	0.0319	0.0343	0.0386	0.0248	0.0221
	$\mathbf{C}  o \mathbf{P}$	0.2052	0.2078	0.1941	0.1395	0.1346
ImageCLEF-DA	$\mathrm{I} \to \mathrm{C}$	0.0088	0.0103	0.0076	0.0103	0.0079
IlliageCLEF-DA	$\mathrm{I} \to \mathrm{P}$	0.1141	0.1131	0.1609	0.1227	0.1126
	$P \rightarrow C$	0.0094	0.0112	0.0079	0.0084	0.0090
	$\mathbf{P} \to \mathbf{I}$	0.0127	0.0141	0.0190	0.0131	0.0134
	Avg.	0.0637	0.0651	0.0714	0.0531	0.0499
	$Ar \rightarrow Cl$	0.2823	0.2860	0.2871	0.2825	0.2777
	$\text{Ar} \rightarrow \text{Pr}$	0.1320	0.1353	0.1219	0.1328	0.1313
	$\text{Ar} \rightarrow \text{Rw}$	0.0782	0.0835	0.1073	0.0820	0.0810
	$Cl \rightarrow Ar$	0.2421	0.2450	0.2503	0.2971	0.2218
	$Cl \rightarrow Pr$	0.1489	0.1517	0.1336	0.1708	0.1354
Office-Home	$Cl \rightarrow Rw$	0.1366	0.1384	0.1412	0.1595	0.1241
Office-Home	$\text{Pr} \rightarrow \text{Ar}$	0.2355	0.2453	0.2580	0.2715	0.2425
	Pr  o Cl	0.3417	0.3419	0.3180	0.3390	0.3257
	$\text{Pr} \rightarrow \text{Rw}$	0.0836	0.0875	0.1007	0.0952	0.0781
	$Rw \to Ar$	0.1439	0.1487	0.1785	0.1750	0.1391
	$Rw \to Cl$	0.2826	0.2812	0.2762	0.2760	0.2613
	$Rw \to Pr$	0.0693	0.0713	0.0725	0.0890	0.0637
	Avg.	0.1814	0.1846	0.1871	0.1971	0.1735
VisDA-2017	$T\toV$	0.3327	0.3312	0.3494	0.3090	0.2916

Pseudo-label generation via DSAN: To obtain pseudo labels, we need to further train the neural network using the DSAN algorithm with the following settings: number of training epochs = 20, transfer\_loss\_weight = 0.5, transfer\_loss = LMMD, learning rate = 0.01, weight decay =  $5 \times 10^{-4}$ , momentum = 0.9. lr\_scheduler is enabled with lr\_gamma = 0.0003, lr\_decay = 0.75. A complete comparison for DSAN generated pseudo labels are provided in Table 4.

Table 4: Evaluation of confidence scores based on AURC (DSAN).

Dataset	Task	Maxprob	Ent	Cossim	JMDS	OT Score
	$C \rightarrow I$	0.0301	0.0318	0.0506	0.0258	0.0240
	$\mathbf{C} \to \mathbf{P}$	0.2024	0.2040	0.1913	0.1391	0.1331
Image CLEE DA	$I \rightarrow C$	0.0090	0.0109	0.0084	0.0105	0.0090
ImageCLEF-DA	$I \rightarrow P$	0.1135	0.1120	0.1607	0.1223	0.1119
	$P \rightarrow C$	0.0102	0.0121	0.0075	0.0096	0.0097
	$P \rightarrow I$	0.0136	0.0150	0.0186	0.0140	0.0135
	Avg.	0.0631	0.0643	0.0729	0.536	0.0502
	$Ar \rightarrow Cl$	0.4306	0.4284	0.4170	0.4515	0.3403
	$\text{Ar} \rightarrow \text{Pr}$	0.2745	0.2738	0.2512	0.2849	0.2133
	$\text{Ar} \rightarrow \text{Rw}$	0.1469	0.1493	0.1521	0.1860	0.1157
	$Cl \rightarrow Ar$	0.2600	0.2631	0.2340	0.3228	0.2097
	$Cl \rightarrow Pr$	0.1757	0.1777	0.1612	0.2225	0.1503
Office-Home	$Cl \rightarrow Rw$	0.1834	0.1848	0.1865	0.2246	0.1493
Office-Hoffie	$\text{Pr} \rightarrow \text{Ar}$	0.2371	0.2381	0.2245	0.2776	0.1984
	$\text{Pr} \to \text{Cl}$	0.3139	0.3105	0.3149	0.3302	0.2711
	$\text{Pr} \rightarrow \text{Rw}$	0.0974	0.0992	0.1037	0.1250	0.0817
	$Rw \to Ar$	0.1301	0.1318	0.1268	0.1751	0.1023
	$Rw \to Cl$	0.2581	0.2555	0.2641	0.2718	0.2112
	$Rw \to Pr$	0.0681	0.0684	0.0628	0.1026	0.0561
	Avg.	0.2146	0.2150	0.2082	0.2478	0.1749
VisDA-2017	$T\toV$	0.2301	0.2290	0.2289	0.2296	0.1799

### **D.1** Binary Toy Examples

To check the effectiveness of the OT score, we consider the binary classification DA task using USPS and MNIST datasets. When testing with the target dataset, we use both (1) the clean data and (2) the data set perturbed with Gaussian noise  $\mathcal{N}(0,\sigma^2I)$ , where we set  $\sigma=0.4$  in our experiments. For each considered task, we compare (1) the accuracy using the pretrained NN on the source domain, (2) accuracy after using semi-discrete OT for domain adaptation, (3) accuracy after eliminating the 10% data with lowest confidence estimated by the OT score. As shown as in Tables 5 and 6, SDOT-DA algorithm improves the performance of the classification network and the OT score can help us eliminate the uncertain data and further improve the accuracy. We also test on difficult pairs of digits and show the result in Table 7.

Tasks	Methods	$\sigma = 0$	$\sigma = 0.4$	Tasks	Methods	$\sigma = 0$	$\sigma = 0.4$
	Original	93.0	93.3		Original	97.1	94.8
0, 1	After OT	98.9	95.4	0, 6	After OT	97.2	95.3
	Quantile 0.1	99.9	96.8		Quantile 0.1	99.4	97.9
	Original	98.3	91.0		Original	96.1	89.2
0, 2	After OT	98.7	96.0	0, 7	After OT	96.2	89.4
	Quantile 0.1	100.0	98.8	]	Quantile 0.1	98.8	93.6
	Original	99.4	96.3		Original	98.6	95.7
0, 3	After OT	99.4	97.8	0, 8	After OT	99.0	96.5
	Quantile 0.1	100.0	99.7		Quantile 0.1	100.0	99.1
	Original	98.8	84.8		Original	92.5	83.1
0, 4	After OT	99.0	92.7	0, 9	After OT	96.3	91.7
	Quantile 0.1	100.0	96.0		Quantile 0.1	98.4	94.3
	Original	98.5	93.5		Original	96.9	91.3
0, 5	After OT	98.8	96.3	Average	After OT	98.2	94.6
	Quantile 0.1	100.0	99.5		Quantile 0.1	99.6	97.3

Table 5: Accuracy for Binary Classification Tasks (USPS → MNIST)

Tasks	Methods	$\sigma = 0$	$\sigma = 0.4$	Tasks	Methods	$\sigma = 0$	$\sigma = 0.4$
	Original	99.8	92.4		Original	99.4	92.8
0, 1	After OT	99.8	95.5	0, 6	After OT	99.6	93.8
	Quantile 0.1	100.0	98.4		Quantile 0.1	100.0	97.7
	Original	99.4	94.2		Original	70.9	70.9
0, 2	After OT	99.4	96.5	0, 7	After OT	99.0	97.2
	Quantile 0.1	100.0	98.8		Quantile 0.1	99.8	99.1
	Original	99.2	96.5		Original	98.6	83.6
0, 3	After OT	99.6	97.7	0, 8	After OT	99.2	92.6
	Quantile 0.1	100.0	99.6	]	Quantile 0.1	100.0	96.5
	Original	99.1	93.9		Original	99.6	92.7
0, 4	After OT	99.8	94.3	0, 9	After OT	99.6	94.0
	Quantile 0.1	100.0	98.6		Quantile 0.1	100.0	98.5
	Original	99.2	89.9		Original	96.1	89.7
0, 5	After OT	99.4	94.0	Average	After OT	99.5	95.1
	Quantile 0.1	100.0	97.9		Quantile 0.1	100.0	98.3

Table 6: Accuracy for Binary Classification Tasks (MNIST → USPS)

$USPS \to MNIST$			$MNIST \to USPS$				
Tasks	Methods	$\sigma = 0$	$\sigma = 0.4$	Tasks Methods $\sigma = 0$ $\sigma =$			$\sigma = 0.4$
	Original	97.1	94.8		Original	99.4	92.8
0, 6	After OT	97.2	95.3	0, 6	After OT	99.6	93.8
	Quantile 0.1	99.4	97.9	1	Quantile 0.1	100.0	97.7
	Original	92.5	83.1		Original	99.6	92.7
0, 9	After OT	96.3	91.7	0, 9	After OT	99.6	94.0
	Quantile 0.1	98.4	94.3	1	Quantile 0.1	100.0	98.5
	Original	87.7	79.7		Original	64.2	64.2
1, 7	After OT	96.6	85.0	1, 7	After OT	98.7	91.5
	Quantile 0.1	98.9	90.0		Quantile 0.1	100.0	95.6
	Original	98.7	94.2		Original	99.4	94.5
2, 3	After OT	98.8	95.2	2, 3	After OT	99.7	95.6
	Quantile 0.1	100.0	98.4	1	Quantile 0.1	100.0	98.8
	Original	98.5	95.7	2, 5	Original	99.4	93.0
2, 5	After OT	98.8	96.2		After OT	99.7	93.8
	Quantile 0.1	100.0	98.5		Quantile 0.1	100.0	98.4
	Original	98.4	88.5		Original	99.0	93.7
3, 8	After OT	98.8	93.9	3, 8	After OT	99.6	93.7
	Quantile 0.1	100.0	98.3		Quantile 0.1	100.0	98.3
	Original	98.9	89.2		Original	98.9	93.2
4, 6	After OT	99.0	92.8	4, 6	After OT	99.1	95.1
	Quantile 0.1	99.9	96.0	1	Quantile 0.1	99.6	97.3
	Original	98.3	84.6		Original	99.4	93.3
5, 6	After OT	98.5	92.5	5, 6	After OT	99.4	93.6
	Quantile 0.1	99.7	96.5		Quantile 0.1	100.0	97.5
	Original	96.3	83.4		Original	99.7	89.6
6, 9	After OT	98.3	94.7	6, 9	After OT	100.0	96.2
	Quantile 0.1	99.9	97.6	1	Quantile 0.1	100.0	99.7
	Original	96.3	88.1		Original	95.4	89.7
Average	After OT	98.0	93.0	Average	After OT	99.5	94.1
	Quantile 0.1	99.6	96.4	1	Quantile 0.1	99.9	98.0

Table 7: Accuracy for Hard Binary Classification Tasks

### D.2 SDOT-DA

We test our SDOTDA algorithm on Digit recognition and Office-31 datasets. In our experiments, we assume the true proportions of each class. In the domain adaptation step, for each class in the source

distribution, we use only the mean feature of that class for computation, which avoids the problem of storing the entire source dataset. As demonstrated from Tables 8 and 9, our SDOTDA algorithm significantly improves the accuracy on the given domain adaptation tasks.

Method	$\mathcal{M}  o \mathcal{U}$	$\mathcal{U} \to \mathcal{M}$
GtA	92.8	90.8
ADDA	89.4	90.1
SRADA	94.1	98.0
RevGrad	77.1	73.0
DRCN	91.8	73.7
ETD	96.4	96.3
Source Only	90.1	80.2
SDOTDA	0.9711	91.22.

Table 8: Accuracy for Classification Tasks Using Semi-Discrete  $OT(USPS \rightarrow MNIST)$ 

Method	$\mathcal{A}  o \mathcal{W}$	$\mathcal{D} \to \mathcal{W}$	$\mathcal{W} \to \mathcal{D}$	$\mathcal{A} \to \mathcal{D}$	$\mathcal{D} \to \mathcal{A}$	$\mathcal{W} \to \mathcal{A}$	Average
Source Only	75.2	91.8	98.8	79.7	62.0	64.4	78.6
SDOTDA	82.6	95.0	99.4	87.8	65.9	66.6	82.9

Table 9: Office-31 Classification